

Cascades and Reconnection in Interacting Vortex Filaments

Rodolfo Ostilla-Mónico,¹ Ryan McKeown,² Michael P. Brenner,² Shmuel M. Rubinstein,² and Alain Pumir^{3,4}

¹*Department of Mechanical Engineering, University of Houston, Houston, TX 77204, USA*

²*School of Engineering and Applied Sciences, Harvard University, Cambridge, MA 02138, USA*

³*Université de Lyon, ENS de Lyon, Université Claude Bernard, CNRS, Laboratoire de Physique, 69342 Lyon, France*

⁴*Max Planck Institute for Dynamics and Self-Organization, 37077 Göttingen, Germany*

(Dated: February 23, 2021)

At high Reynolds number, the interaction between two vortex tubes leads to intense velocity gradients, which are at the heart of fluid turbulence. This vorticity amplification comes about through two different instability mechanisms of the initial vortex tubes, assumed anti-parallel and with a mirror plane of symmetry. At moderate Reynolds number, the tubes destabilize via a Crow instability, with the nonlinear development leading to strong flattening of the cores into thin sheets. These sheets then break down into filaments which can repeat the process. At higher Reynolds number, the instability proceeds via the elliptical instability, producing vortex tubes that are perpendicular to the original tube directions. In this work, we demonstrate that these same transition between Crow and Elliptical instability occurs at moderate Reynolds number when we vary the initial *angle* β between two straight vortex tubes. We demonstrate that when the angle between the two tubes is close to $\pi/2$, the interaction between tubes leads to the formation of thin vortex sheets. The subsequent breakdown of these sheets involves a twisting of the paired sheets, followed by the appearance of a localized cloud of small scale vortex structures. At smaller values of the angle β between the two tubes, the breakdown mechanism changes to an elliptic cascade-like mechanism. Whereas the interaction of two vortices depends on the initial condition, the rapid formation of fine-scales vortex structures appears to be a robust feature, possibly universal at very high Reynolds numbers.

I. INTRODUCTION

Many experiments have demonstrated that the interaction of two vortex tubes coming close together eventually leads to a change of topology of the vortex lines through a process known as vortex reconnection [1–3]. Vortex reconnection is a fundamental process in fluid mechanics, and it has been postulated to play a significant role in fluid phenomena such as the turbulent energy cascade [4], noise generation [5] and the transfer of helicity across topologically distinct vortices [6]. Reconnection is also interesting from a theoretical point of view, as the change of vortex line topology appears to violate well-known conservation theorems in inviscid flows [7], which implies that viscosity must play a decisive role even at extreme Reynolds numbers.

The process through which vortex pairs undergo reconnection has been well studied and characterized both numerically and theoretically. The early phase of the interaction, before viscosity plays the dominant role, is captured by the Biot-Savart equation, which keeps track of the location of the vortex tubes by assuming a circular structure of the cores, with a fixed vorticity profile [8]. The numerical work of [9] showed that the resulting dynamics of a wide range of initial conditions spontaneously leads to the local pairing of antiparallel parts of nearby filaments. As a result, the cores get close together, which generally leads to very rich dynamics. The Biot-Savart description, however, fails when the vortex tubes are so close that they deform each others' cores, thereby making the initial assumption questionable [10, 11]. Therefore, to adequately capture the initial dynamics of the interaction, it is necessary to undertake a full simulation of the Euler

equations. The Biot-Savart equation (and the Euler equations) also fail to capture the viscous processes, essential to reconnection, which occur at scales much smaller than any other inviscid process scale [11].

It has been known for a long time that several instability mechanisms may lead to the disruption of two antiparallel vortex lines. Early studies based on the Biot-Savart equation suggested that the long-wavelength Crow-instability [12] plays the dominant role in bringing together counter-rotating parts of the tubes so reconnection can occur [13, 14]. This prompted a number of investigations, see e.g.[5, 15–20], based on numerical solutions of the Euler and Navier-Stokes equations which imposed the symmetry of the most unstable mode corresponding to the long wave-number Crow instability, namely that of two tubes with two mirror symmetry in the plane that separates them (denoted as the plane P_1). With this symmetry, the components of velocity perpendicular to the plane P_1 is uniformly zero, so if the vorticity component perpendicular to the plane is zero, then, reconnection is impossible in the absence of viscosity. The observation that the time necessary to achieve reconnection, in the limit of very small viscosity, ν , seems in practice to be independent of viscosity, suggests that the limit $\nu \rightarrow 0$ [11] (or alternatively, of the limit $Re_\Gamma \rightarrow \infty$, where Re_Γ , the Reynolds number is defined as $Re_\Gamma = \Gamma/\nu$, Γ being the circulation of the vortex tubes and ν the kinematic viscosity) is singular. This observation has been interpreted as a signature pointing to the existence of singular solutions of the Euler equations. The study of simplified models, based on the Biot-Savart equations, has suggested a large amplification of vorticity during the late stages of reconnection, although the approximations necessary to derive the Biot-Savart model ultimately break down [13, 21, 22]. Furthermore, decades of careful numerical work have not conclusively resolved the singularity issue for the corresponding initial value problem. The problem has been particularly studied in the inviscid limit, looking for signs of a diverging vorticity [15, 17, 18]. Still, DNS clearly show that very thin vortex sheets are formed on either side of the symmetry plane P_1 , both in the inviscid and in the viscous problem at large enough Re_Γ . The formation of extremely thin vortex sheets, with a relatively slow growth of vorticity makes the problem very difficult to study numerically.

While the quest to reach increasingly large values of Re_Γ continues [23], numerical and experimental studies have recently identified another main mechanism in the interaction between two antiparallel tubes, which leads to the breaking of the vortex tubes instead of to a reconnection [24]. This mechanism can be observed in the head-on collision between two vortex rings, which leads to a very rapid destruction of the vortices at large Reynolds numbers [25]. In this problem, the long-wavelength Crow instability initially brings parts of the filaments together [26, 27]. However, the further interaction between the counter-rotating tubes, reveals the dominant role of an instability whose wavenumber is comparable with the core size [28, 29]. This instability, known as the elliptic instability [26, 30, 31], involves a symmetry that completely differs from that of the long-wavenumber Crow instability. At sufficiently high Reynolds numbers, elliptic instabilities develop on top of each other, leading to a cascade, and eventually, to a transient turbulent flow [24].

The marked difference between these two cases leads us to investigate the onset of the mechanisms leading to reconnection. In this vein, we take inspiration from the studies of reconnecting magnetic tubes at an angle in an astrophysical context [32], and from the recent study of vortex reconnection in superfluids, which has revealed the presence of non-universal features by comparing different classes of initial conditions [33]. However, we have to highlight the notable difference between these two cases, and ours, which arises from much larger degrees of freedom of the vortex cores in hydrodynamics and leads to a much richer phenomenology, not taken into account in the simplified model of reconnection of skewed vortices in [34]. While it is clear that reconnections are still present in hydrodynamical fluids with $Re_\Gamma \gg 1$ [23], their appearance could be restricted to a rather small subset of initial conditions that either enforce many symmetries on the vortices or stabilize the core through spin [20]. This would mean that reconnections (understood as topological

changes) become rare in a classical fluid and play a small role in the conveyance of energy across scales, even if they remain important from a theoretical and mathematical perspective [35].

We address the question about genericity by relaxing some of the strict symmetries imposed on the usual reconnection studies. We perform a series of direct numerical simulations which use the simple configuration of two counter-rotating vortex tubes oriented at an angle as the initial condition. We work at a Reynolds number where for antiparallel tubes, the elliptical instability dominates, due to the amplification of strain that results from their alignment. We start off with two filaments which are perpendicular to each other. For this configuration, we will see that the strain orientation does not excite the elliptical instability. We then vary the angle, making the vortices more antiparallel and recover the elliptical instability. In practice, we use $b = \cot(\beta/2)$, where β is the angle between the filaments. With this choice, $b = 1$ corresponds to two initially perpendicular filaments: $\beta = \pi/2$. In this study, we consider only values of $\beta \leq \pi/2$ ($b \geq 1$), thus favoring configurations where the two filaments tend to be initially counter-rotating, rather than co-rotating. We note that the configuration $\beta = \pi/2$ ($b = 1$) has been studied, originally at much smaller Reynolds numbers than the ones considered here and with an additional hyperviscous dissipation term [36], and more recently at a much higher resolution [37].

In all cases, we find an energy cascade during the interaction, reaching ever smaller scales as the Reynolds number increases. This generation of small scales arises from deformations of the cores where the tubes intersect. We find that the interaction starts with the formation of characteristic vortex sheets for $67.4^\circ \leq \beta \leq 90^\circ$ ($1 \leq b \leq 3/2$). For $\beta \leq 53.1^\circ$ ($b \geq 2$), however, the mechanism that prevails in the interaction between the two tubes is the formation of transverse vortex tubes, as observed, formally, when $\beta \rightarrow 0$ ($b \rightarrow \infty$) due to the presence of the elliptical instability [24].

II. NUMERICAL PROCEDURES AND DATABASE

We simulate the incompressible Navier-Stokes equations:

$$\partial_t \mathbf{u} + (\mathbf{u} \cdot \nabla) \mathbf{u} = -\rho^{-1} \nabla p + \nu \nabla^2 \mathbf{u} \quad (1)$$

$$\nabla \cdot \mathbf{u} = 0 \quad (2)$$

in a triply periodic box, using pseudo-spectral methods. The details of the code have been described in [38]. We vary the aspect ratio of the domain, which we take to be of size 2π in the x and y direction, and of size $2b\pi$ in the z direction, where b is a control parameter that we take as $b = 1, 5/4, 3/2, 2, 5/2, 3, \text{ and } 4$. No forcing is added to the Navier-Stokes equations, and the flow is allowed to evolve from the initial conditions. These consist of two Gaussian vortices, where the initial position of the vortex cores are in two diagonal lines $\gamma_\pm z = \pm bx$ located at the plane $y = \pm d/2$. The vorticity is initially concentrated around the two lines, with a Gaussian distribution: $\omega_\pm(\mathbf{x}, t = 0) = \pm \Omega \exp(-\rho_\pm^2/2\sigma^2)(e_x \pm be_z)/\sqrt{1+b^2}$, where ρ_\pm is the distance between the point \mathbf{x} to the two lines γ_\pm , and σ is the core radius. The resulting circulations, Γ_\pm , are equal to $\Omega\sigma^2$. A schematic of the initial condition can be seen in Fig. 1, which shows that the iso-contours of vorticity approximately concentrate in two tubes, at an angle of inclination $\beta = 2 \arctan(1/b)$.

Our calculations are organized in two series of runs. In the first series, we fix the angle by setting $b = 1$, which results in $\beta = 90^\circ$ to each other. This configuration minimizes the strain direction that triggers the elliptical instability. We then vary the Reynolds number, from $Re_\Gamma = 2200$ to $Re_\Gamma = 5400$, which is around the Reynolds number range for which the elliptical instability supersedes the Crow instability for antiparallel tubes, to study the genericity of the elliptical instability in the most disadvantageous configuration. In the second series of runs, we fix the Reynolds number at $Re_\Gamma = 4000$, and vary b from 1 to 4, which reduces the angle, β , and brings

Runs	1	2	3	4	5	6	7	8	9	10	11	12A/B/C
b	1	1	1	1	1	5/4	3/2	2	5/2	3	4	∞
β	90°	90°	90°	90°	90°	77.3°	67.4°	53.1°	43.6°	36.8°	28.1°	0°
Re_Γ	2200	3300	4000	4550	5400	4000	4000	4000	4000	4000	4000	4000
N_l	256	256	384	384	384	192	240	192	192	192	192	192*
N_h	384	512	512	512	512	384	400	320	320	320	320	320*

TABLE I. Simulation parameters for the runs used in this work. The numerical domain is taken as $-\pi \leq x \leq \pi$, $-\pi \leq y \leq \pi$ and $-b\pi \leq z \leq b\pi$. The Reynolds number is defined as the ratio of the initial circulation, Γ , divided by the kinematic viscosity, ν . Each run was started at low resolution, with $N_l \times N_l \times bN_l$ Fourier modes. The runs were also conducted at a higher resolution, with $N_h \times N_h \times bN_h$ Fourier modes during the generation of small-scale flow structures. *For these cases with $\beta = 0^\circ$, the limits in the z direction are taken as $-4\pi \leq z \leq 4\pi$, and the z resolution is accordingly $4N_l$ or $4N_h$.

the tubes closer to being antiparallel, progressively amplifying the strain in the direction that induces the elliptical instability.

In addition, we considered 3 runs with initially antiparallel vortex tubes, in the configuration studied in [24, 27]. These runs were carried out in a box of aspect ratio 4, although they correspond formally to $\beta = 0$, hence $b \rightarrow \infty$. In these runs, we kept the Reynolds number to $Re_\Gamma = 4000$, and we slightly modulated the constant x and y -locations of the tubes by a sum of a few Fourier modes. We varied the overall coefficient of the perturbation by multiplying by 2 and 4. The runs were carried out at low resolution ($192^2 \times 768$). Complementary runs at higher resolution convinced us that the low resolution was in fact sufficient.

In all the runs, the initial evolution is relatively smooth and does not require a very high resolution. We have therefore started all the runs at a low resolution, with a grid of size $N_l \times N_l \times (bN_l)$ (or equivalently, with as many Fourier modes). When the vortex tubes come together, the velocity field develops very fine scales, or equivalently, the Fourier spectrum extends to much larger values of the wavenumbers, k . To simulate this phase of the dynamics, we extend the number of Fourier modes to $N_h \times N_h \times (N_h b)$. The parameters of the various simulations are shown in Table I.

In the following, all quantities will be expressed in units defined with the box-size and a unitary circulation. Note that the time scale associated with the inviscid evolution (Biot-Savart model) is $\sim d^2/\Gamma$, which is of order 1.

Symmetries of the problem: Although the planes P_1 ($z = 0$) and P_2 ($y = 0$), as indicated in Fig. 1, play a particularly important role in the problem studied here, the velocity and vorticity fields in our simulations do not have any simple symmetry with respect to P_1 or P_2 . In configurations with a symmetry with respect to P_1 , as it is the case e.g. in [11, 15–20, 39, 40], the component of the velocity field perpendicular to P_1 is equal to 0 in P_1 . As a consequence of this symmetry, if the component of vorticity perpendicular to P_1 is initially 0 in the symmetry plane P_1 , then, a component of vorticity perpendicular to P_1 cannot be generated without viscosity.

Conversely, there is no particular symmetry plane between two vortex tubes undergoing the elliptic instability [24, 27], or in the configuration of two vortex tubes initially at a finite angle. Nonetheless, the fields in the present study are invariant after composing the two mirror symmetries with respect to P_1 and to P_2 , or equivalently, by a rotation with respect their intersection, i.e. the straight line Δ ($z = y = 0$) shown in Fig. 1(a). This corresponds to the following symmetry:

$$(x, y, z) \rightarrow (x, -y, -z), \quad (u_x, u_y, u_z) \rightarrow (u_x, -u_y, -u_z) \quad \text{and} \quad (\omega_x, \omega_y, \omega_z) \rightarrow (\omega_x, -\omega_y, -\omega_z) \quad (3)$$

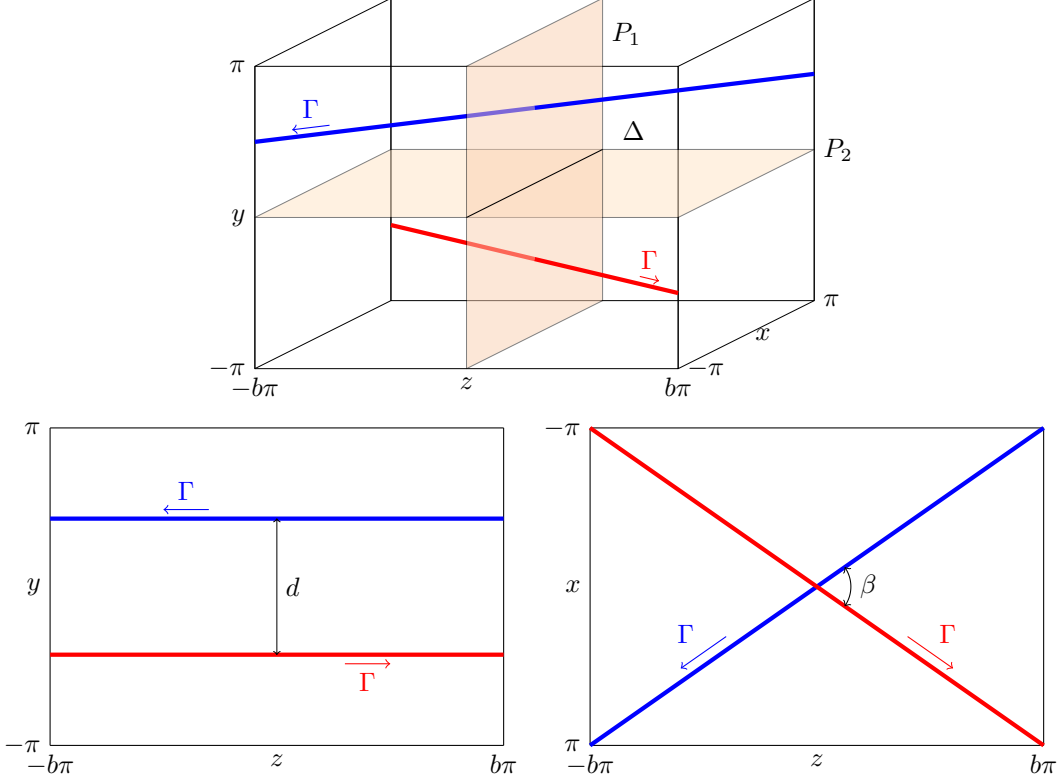


FIG. 1. Schematic of DNS initial configuration. The thick red and blue lines represent the initial positions of the two vortex filaments, with the arrow indicating the circulation direction. (a) 3D schematic. (b) side view of the yz -plane, which shows the definition of the spacing between the filaments, d . (c) top view of the xz -plane, which shows the definition of β and b . The vorticity distribution is invariant under the symmetry resulting from two mirror symmetries with respect to the planes P_1 and P_2 : $(x, y, z) \rightarrow (x, -y, -z)$; $(\omega_x, \omega_y, \omega_z) \rightarrow (\omega_x, -\omega_y, -\omega_z)$ and $(u_x, u_y, u_z) \rightarrow (u_x, -u_y, -u_z)$. The distance between the two tubes in the y direction is $d = 0.9$; the circulation is chosen here to be $\Gamma = 1$, and the core radius $\sigma = 0.4/\sqrt{2} \approx 0.28$.

III. RESULTS

A. Overview of reconnection

We begin by illustrating the phenomenon of reconnection for initially perpendicular vortex tubes by analyzing run 3, with $\beta = 90^\circ$ ($b = 1$), $Re_\Gamma = 4000$. The vortices evolve in time from the initial horizontal conditions, as they approach one another and begin to deform. Fig. 2(a) shows the vorticity isosurface at $t = 15.2$, before the reconnection event. As the flow evolves further, the vortices reconnect. This results in a changed topology, which can be inferred from the structure of the vorticity field shown in panel (b) at $t = 26.4$. Vertical vortex structures, however, appear simultaneously with smaller scale, horizontal filaments perpendicular to the main tubes. To better characterize the large scale flow structures, present before and after reconnection, we use the methods applied by Goto et al. [42], which consists of band-pass filtering the vorticity field. For the purpose of the present work, we found it convenient to isolate the wavenumbers in the band defined by $\sqrt{2}k_f \leq k \leq 2\sqrt{2}k_f$, where $k_f = 2.3$. This filters out the small-scale features clearly seen in panel (a,b), but leaves apparent the change of topology due to the evolution: the originally horizontal tubes, parallel to the z axis in Fig.2(c), become parallel to the y axis at later

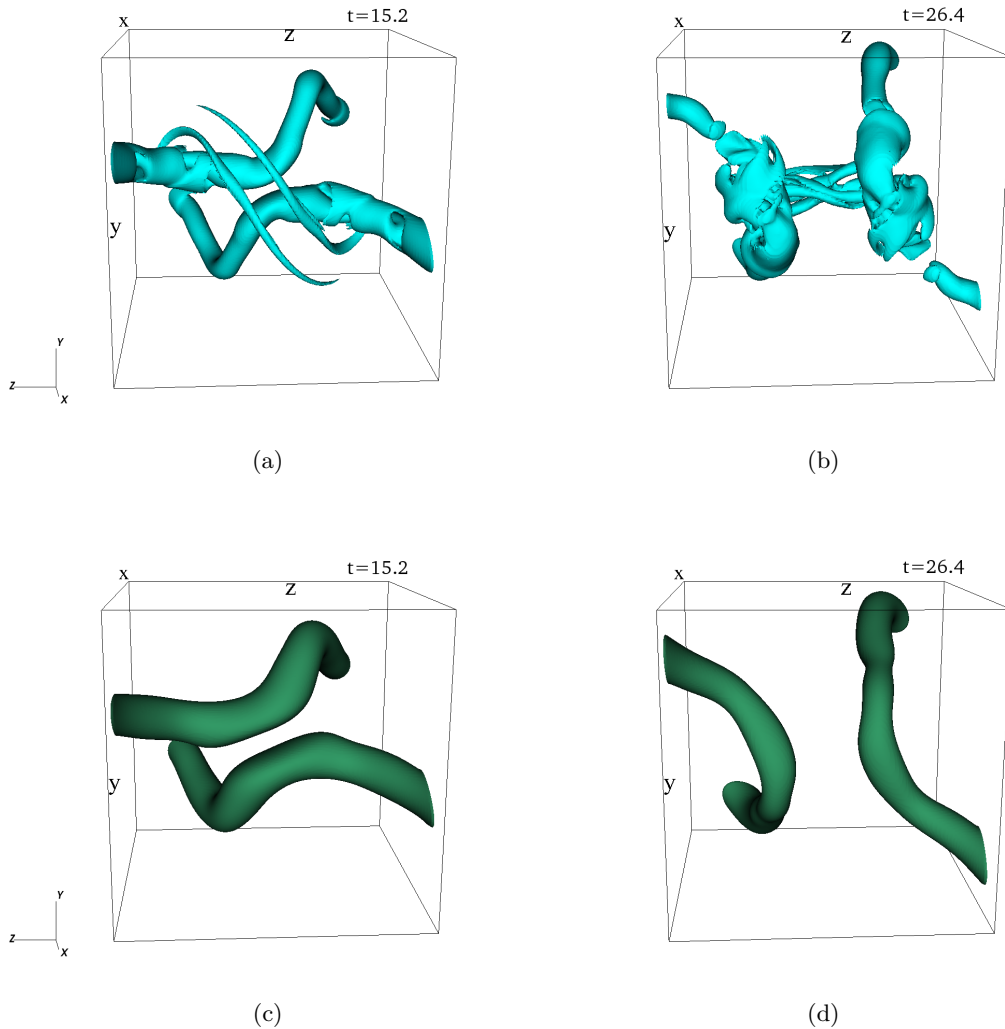


FIG. 2. Vortex topology changes during a reconnection between initially perpendicular vortex tubes ($b = 1$ and $Re_{\Gamma} = 4000$, run 3 in Table I). Panels (a) and (b) show iso-vorticity contours corresponding to $\omega_{th} = 2.5$ at $t = 15.2$, when the tubes begin to interact, and at $t = 26.4$, after the interaction. These dynamics reveal a change of topology of the vortex lines and the generation of small-scale vortices during the reconnection. Panels (c) and (d) show the same vorticity field, band-pass filtered between $k_{<} = \sqrt{2}k_f$ and $k_{>} = 2\sqrt{2}k_f$, with $k_f = 2.3$, which removes the small-scale features of the flow and showcases only the change of topology of the vortex tubes. The value of the isosurface is 1 in panels (c) and (d). Full videos of the process are available as supplementary material [41].

times (see Fig. 2(d)), signaling a topological transition in the vorticity field. Between the two times shown in panels (a) and (b), we can observe not only changes in the large-scale vortex topology, but also the progressive appearance of small-scale vortical flow structures. At early times, we can observe the appearance of slender vortex filaments which are perpendicular to the primary vortex tubes and contain little circulation. These filaments are a well-known feature of reconnection which has already been discussed in previous studies, usually under the name of bridges [43–45]. In our simulation, they are clearly visible at $t = 15.2$, Fig. 2(a). While the vorticity in the bridges is very much amplified at early times through vortex stretching, the role that these slender filaments

have in the subsequent interaction of the main tubes during reconnection appears to be limited because they contain little circulation. Conversely, the small scale features clearly visible at later times ($t = 26.4$, Fig. 2(b)) appear to be a reproducible feature of the interaction at high Reynolds numbers; recent DNS of a pair of vortex tubes, with imposed symmetry with respect to planes P_1 and P_2 (in our terminology), also led to the formation of a similar small scale structures, which was interpreted to be the result of a cascade [20].

The reconnection process between two vortex tubes initially at an angle $\beta = 90^\circ$, illustrated in Fig. 2, exhibits similarities with reconnection of two tubes with symmetric initial conditions [11, 20], as noted e.g. in [36], and explained in more detail below. The dynamics leading to reconnection, however, are *not* universal. In fact, Fig. 3 shows an overview of the interaction between two tubes initially at a much shallower angle, $\beta \approx 28.1^\circ$ ($b = 4$, run 11). Fig. 3(a) shows that the interaction occurs over two closely paired sections of the vortex tubes. This is clearly illustrated by Figs. 3(c) and (d), which show iso-vorticity contours of the band-pass filtered solution for $\sqrt{2}k_F \leq k \leq 2\sqrt{2}k_F$, with $k_F = 2.3$, as shown in Figs. 2(c) and (d). The configuration with $\beta = 28.1^\circ$ ($b = 4$) exhibits a different type of dynamics, resulting in a larger portion of the vortices coming closer to each other than at $\beta = 90^\circ$ ($b = 1$). The collision between these vortex tubes leaves behind a tangle of smaller vortices, reminiscent of the breakdown that results from the collision of two vortex rings [24, 27]. This points to a dependence on the initial orientation angle, which is examined further in the following sections.

B. Evolution of two nearly perpendicular tubes: sheet formation.

Early stage and sheet formation The reconnection process starts with the pairing of the tubes, which locally aligns the vortices in an antiparallel manner, a feature clearly observed directly from the Biot-Savart equation [9], and consistent with all previous numerical observations. The local pairing of antiparallel filaments is accompanied by a significant deformation of the vortex tubes. Fig. 4(a-c) shows iso-surfaces of the vorticity magnitude for $\beta = 90^\circ$ and $Re_\Gamma = 4000$ to illustrate this interaction. The three views from a perspective similar to that shown in Fig. 1(a), at $t = 17$ (Fig. 4(a)), $t = 19$ (Fig. 4(b)) and $t = 20$ (Fig. 4(c)) indicate that the nearest regions of the tubes come together and flatten into thin vortex sheets. It is important to notice that the spatial extent of the vortex sheets, in the direction of the vortex tubes, is in fact rather limited. The vortex sheets are confined in the z -direction to a size smaller than that of the initial vortex cores. We also stress that the sheets do not appear to perfectly align with the P_2 ($y = 0$) plane, as it happens in the canonical problem of two initially weakly perturbed antiparallel vortex tubes, symmetric with respect to the midplane. In fact, the tilt of the sheets increases from $t = 17$ to $t = 20$.

The pairing shown in Fig. 4(a-c) with the formation of vortex sheets in the regions where the vortices interact, is qualitatively consistent with the simulations of [36]. As already stated, the formation of sheets is a robust feature in many simulations of interacting vortex tubes, starting with an initial configuration of almost parallel counter-rotating tubes with a slight perturbation [40]. Further insight on these vortex sheets is provided by Fig. 4(d), which shows a magnified view at $t = 20$, from a slightly different perspective, showcasing the pronounced flattening of the vortex cores. As shown in Fig. 4(e-f), the isocontours of the z component of vorticity at the central plane, $z = 0$ (the plane P_1 , as introduced in Fig. 1(a)) and at an adjacent plane parallel to P_1 which is slightly off the symmetry plane, further indicate the formation of intense, thin vortex sheets. Up to the time shown in Fig. 4(d), the flattening of the sheets is not greatly affected by increasing the Reynolds number. We view this as evidence that the formation of the narrow vortex sheets is only a precursor of reconnection.

We notice that Fig. 4(a-c) also demonstrates that the vortex filament “bridges”, clearly visible

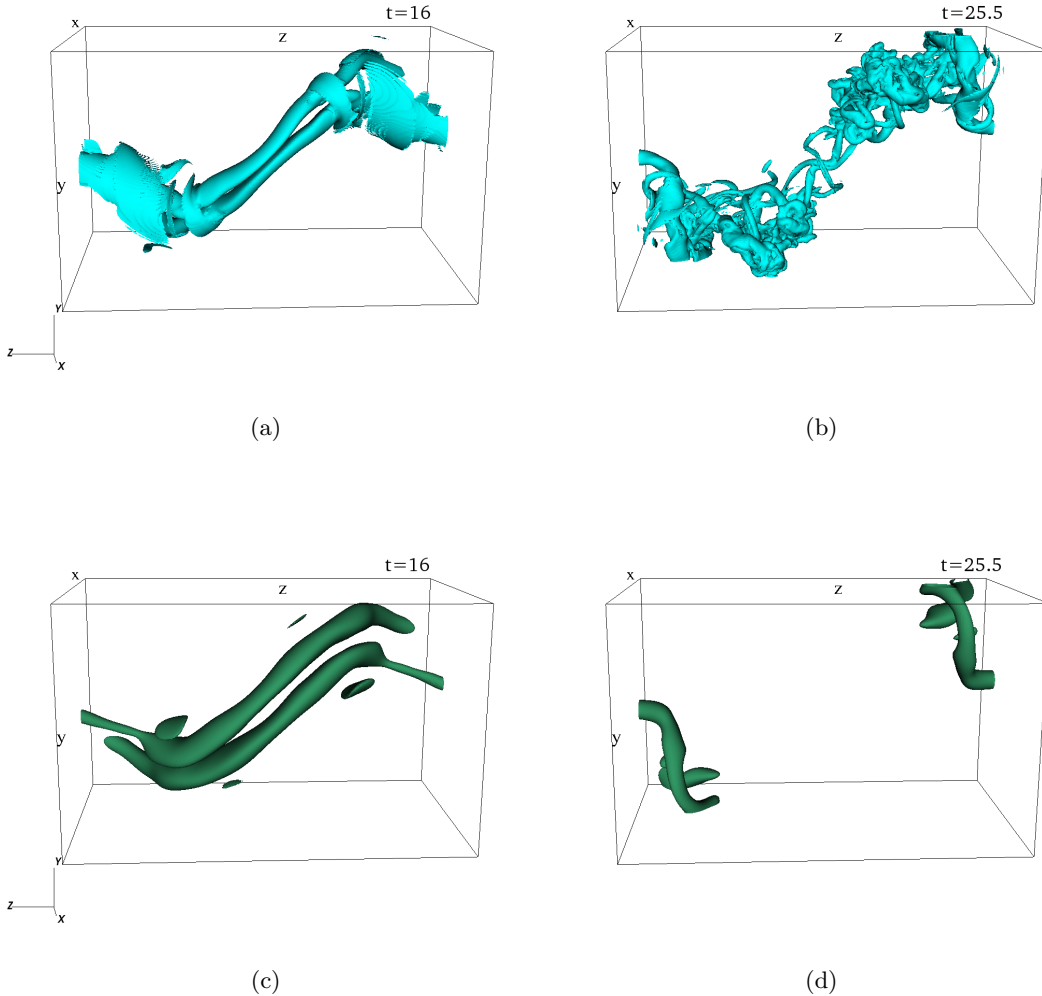


FIG. 3. Vortex topology changes during a reconnection between tubes at an acute angle ($\beta \approx 28.1^\circ$, $b = 4$ and $Re_\Gamma = 4000$, run 11 in Table I). Panels (a) and (b) show iso-vorticity contours corresponding to $\omega_{th} = 2.35$ at $t = 16$, when the tubes are paired, and at $t = 25.5$, after the interaction, respectively. These panels show the generation of fine-scale vortices, similar to the collision of two antiparallel vortices [24]. Panels (c) and (d) show the band-passed vorticity field, between the wavenumbers $k_< = \sqrt{2}k_f$ and $k_> = 2\sqrt{2}k_f$ (where $k_f = 2.3$), at the same times as (a) and (b). The large-scale portions of the vortex tubes at the middle of the interaction zone break down by $t = 25.5$, and the tubes reconnect at the edges of the interaction zone. The value of the isosurface in panels (c) and (d) is 0.85. Full videos of the process are available as supplementary material [41].

at the earlier stages of the interaction when the tubes are drawn closer together, (Fig. 2(a)), are still visible at $t = 17$ (Fig. 4(a)). As the vortex tubes begin to flatten into sheets at $t = 19$ (Fig. 4(b)), these bridges become less pronounced and are no longer present at $t = 20$ (Fig. 4(c)). Part of the reason why the bridges are less visible at later times is the increase in the vorticity threshold, ω_{th} used at the three different times. The vorticity magnitude increases locally at the reconnection site where the cores become locally flattened into sheets. In fact, the bridges are concentrated in very narrow regions of space; this implies that large velocity gradients are generated, but that viscosity

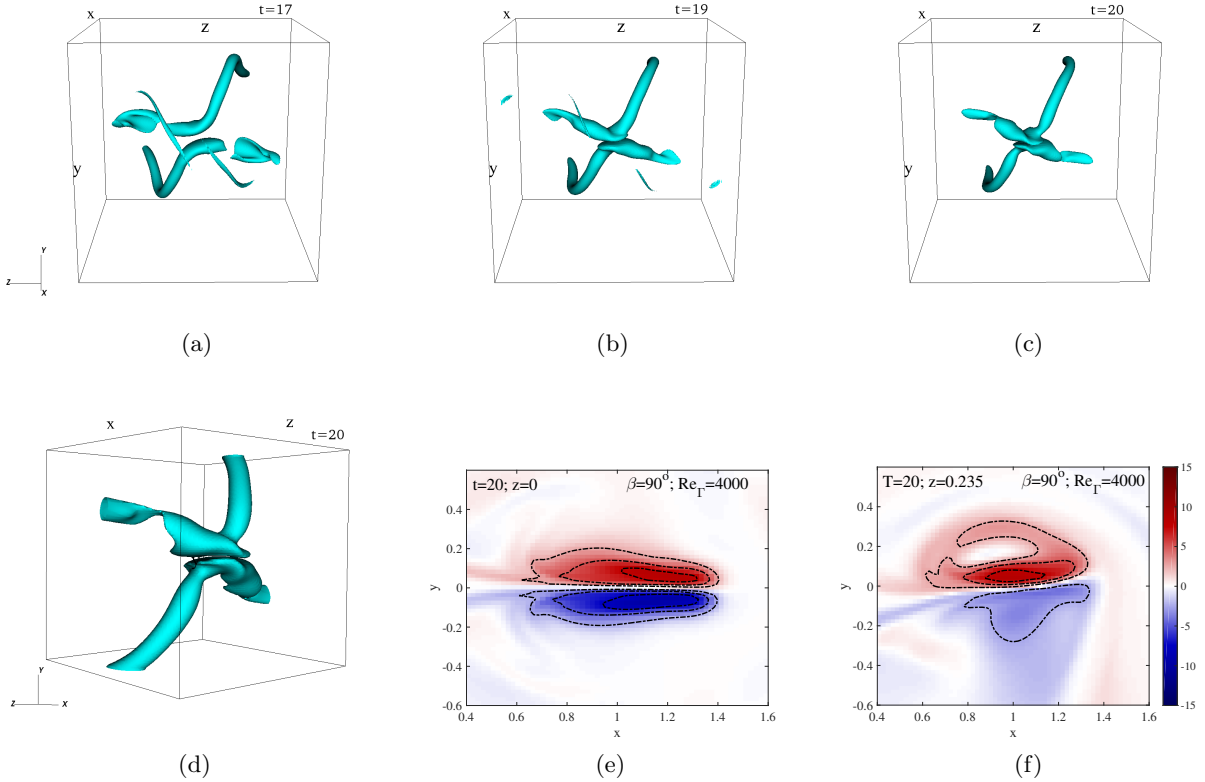


FIG. 4. Close-up view of sheet formation near the reconnection event of initially perpendicular vortex tubes (run 3, $\beta = 90^\circ$, $b = 1$, $Re_\Gamma = 4000$). Iso-vorticity contours of the flow, shown at $t = 17$ (panel (a), $\omega_{th} = 3.6$), $t = 19$ (panel (b), $\omega_{th} = 3.8$) and $t = 20$ (panel (c), $\omega_{th} = 4.0$), reveal the formation of a flattened region of amplified vorticity where the two tubes locally contact. (d) A more detailed view of the region where the vortices interact is shown by zooming in and rotating the domain at $t = 20$, $\omega_{th} = 4.0$. (e-f) Cross-sectional plot of the z -component of vorticity in the middle plane, P_1 at $z = 0$ (panel e) and at $z \approx 0.15$ (panel f).

acts very strongly to dissipate them. For these reasons, as already stated, the bridges do not play any appreciable role in the reconnection dynamics and are immaterial for the present discussion.

Late stage and reconnection The flattening of the cores into sheets is the precursor of the reconnection process. Up until the latest time, shown in Fig. 4(c), the vortex lines are not broken; they are brought together and compressed into a narrow region. The change of topology of the vortex lines, clearly illustrated in Fig. 2, occurs at a later stage through the destruction of the vortex sheets. We stress that this process is strongly constrained by the symmetry imposed, as in the previously studied case of the two initially weakly perturbed, antiparallel vortex tubes (c.f. [20]). With our initial conditions, as previously noted, the sheets do not particularly align with any plane. In fact, as shown in Fig. 5, the vortex sheets strongly deform in a fully 3-dimensional manner at later times. The vortex sheets begin to twist around each other at $t = 21.6$ (Fig. 5(a)), until the sheets, originally aligned mostly parallel to the P_2 ($y = 0$) plane, become almost vertical along the P_1 plane ($z = 0$), as shown in Fig. 5(b). The continued twisting of the vortex sheets causes them to become locally folded along both sides of the P_1 plane, leading to the formation of transverse vortex filaments. Shortly afterward, at $t = 23.2$, shown in Fig. 5(c), the main sheets in the P_1 plane are annihilated, leaving behind a complicated tangle of small-scale vortices. The

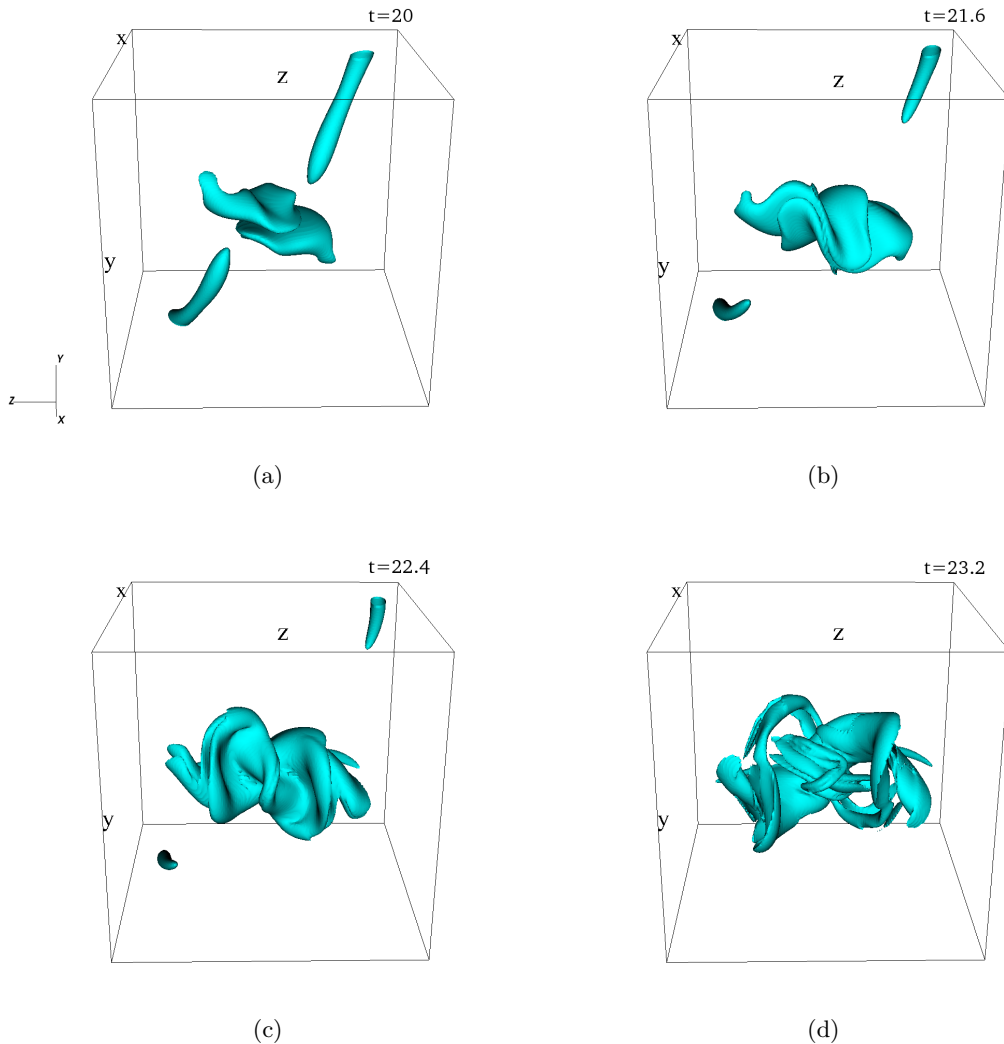


FIG. 5. Twisting of the vortex sheets and reconnection. Vorticity magnitude isosurface for initially perpendicular vortex tubes in run 3 ($\beta = 90^\circ$, $Re_\Gamma = 4000$) at three consecutive times, following the vortex sheet formation. (a) After the vortex cores flatten into sheets, they become twisted as they wrap around each other. (b) The vortex sheets become folded and reorient along the $z = 0$ (P_1) plane, forming an array of transverse vortex filaments. (c) The two strong vortex sheets annihilate, leaving a tangle of small-scale vortex filaments. The last time shown, $t = 23.2$ corresponds approximately to the peak dissipation rate, see Fig. 6(b). The iso-vorticity contours of the flow, are shown at $t = 21.6$ ($\omega_{th} = 5.25$), $t = 22.4$ ($\omega_{th} = 5.60$) and $t = 23.2$ ($\omega_{th} = 6.0$). The plane P_1 ($z = 0$) separates the box shown in the middle.

results of Fig. 5 therefore show that once the vortices pair off and begin to interact, the evolution of the reconnection dynamics differs significantly from those obtained with a much more symmetric initial condition, such as [20] which cannot account for the twisting of the sheets. This difference may affect the formation of small-scale vortices, which form at later times, as shown in Fig. 2(b).

Evolution of global quantities A quantitative measure of the production of small scales during the reconnection process is shown in Fig. 6 for the interaction of initially perpendicular vortex tubes at several Reynolds numbers. Over the entire period of the simulation, the mean kinetic energy rate, shown in Fig. 6(a), decays by less than 20%, despite the rapid increase in the mean

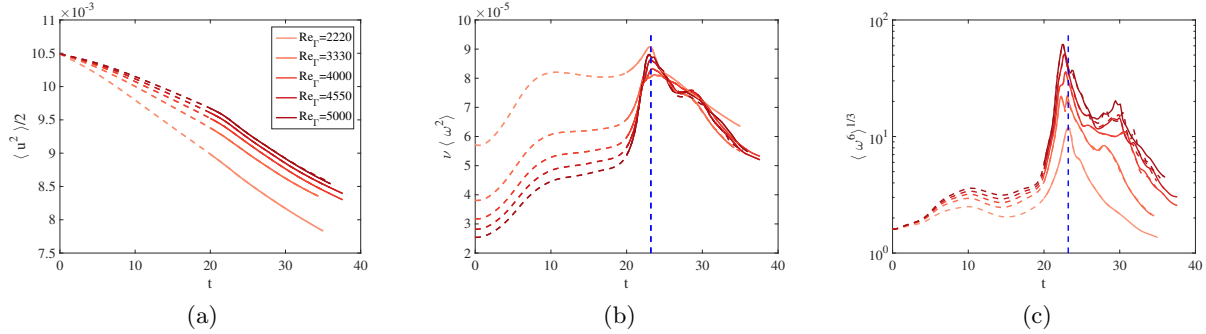


FIG. 6. Global dynamics for initially perpendicular vortex tubes at various Reynolds numbers. The evolution of (a) the mean kinetic energy rate, $\langle \mathbf{u}^2 \rangle / 2$, (b) the mean dissipation rate, $\nu \langle \omega^2 \rangle$, and (c) the mean 6th moment of the vorticity, $\langle \omega^6 \rangle^{1/3}$, for runs 1-5, at fixed $\beta = 90^\circ$ and increasing values of Re_Γ . The vertical dashed line in (b) and (c) corresponds to $t = 23.2$, which is the last time shown in Fig. 5(c), and is also very close to the peak dissipation rate. The dashed (respectively full) lines correspond to runs at low (respectively high) resolutions.

dissipation rate, shown in Fig. 6(b). For each run, the initial mean dissipation rate decreases with a scaling of $\sim 1/Re_\Gamma$ as the Reynolds number increases. It reaches a peak value at a time that is essentially independent of Re_Γ . We note that the peak dissipation time t_{peak} will approximately coincide with the time the small-scale vortices are most energetic, so we can use this time to study the resulting small-scale structure.

Notably, the height of the peak in the dissipation rate does not vary significantly as a function of the Reynolds number. Further information on the generation of motion at small scales is provided by higher moments of the vorticity distribution. Specifically, Fig. 6(c) shows the 6th moment of the vorticity, taken to power 1/3. The 6th moment is defined as:

$$\langle \omega^{2n} \rangle = \frac{1}{V} \int_V d^3 \mathbf{x} (\omega^2)^n \quad \text{where } n = 3 \quad (4)$$

We chose to show a moment of finite order of the vorticity distribution, rather than the maximum of the vorticity, which corresponds to the limit $n \rightarrow \infty$, as the latter is far more sensitive to finite resolution effects.

Since all runs share the same initial condition, the plots of $\langle \omega^6 \rangle^{1/3}$ all start at the same initial value at 0. The peaks of the curves reach increasingly higher values with increasing Re_Γ ; for the $Re_\Gamma = 5000$ case the maximum is approximately 35 times greater than the initial value. This trend reflects the strong amplification of vorticity that occurs during reconnection as the cores contact and break down to fine scales. Similar results are obtained with values of other moments of $\langle \omega^{2n} \rangle^{1/n}$, with $n = 2$ and 4. As expected, the peak amplification for these moments grows with the order n . Note that on all plots in Fig. 6, the results of the runs at low resolution (with N_l^3 Fourier modes) are shown as a dashed lines, whereas the runs at higher resolution (with N_h^3 modes, N_l and N_h both given in Table I) are represented by solid lines. The deviations between the two resolutions are small in the peak regions, even at the highest Reynolds number considered here. This gives us confidence in our numerical results. However, at $Re_\Gamma = 5000$, the values of $\langle \omega^6 \rangle^{1/3}$ at different resolutions diverge at later times (for $t \gtrsim 25$), which we interpret as a consequence of the amplification of small differences in the numerical integration of such a dynamical system with many degrees of freedom and underlying chaotic dynamics.

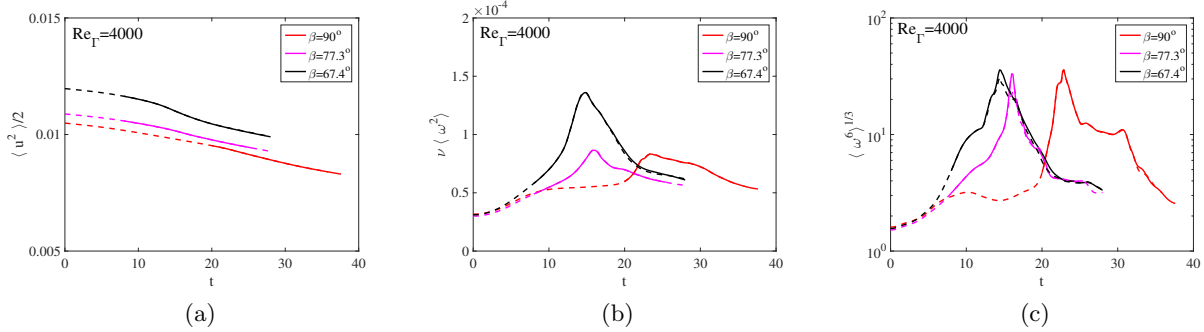


FIG. 7. Global dynamics for vortex tubes at varying initial orientation angles. The evolution of (a) the mean kinetic energy rate, $\langle \mathbf{u}^2 \rangle / 2$, (b) the mean dissipation rate, $\nu \langle \omega^2 \rangle$, and (c) the mean 6th moment of the vorticity, $\langle \omega^6 \rangle^{1/3}$, for runs 3 ($\beta = 90^\circ$, $b = 1$), 6 ($\beta \approx 77.3^\circ$, $b = 5/4$), and 7 ($\beta \approx 67.4^\circ$, $b = 3/2$), at fixed $Re_\Gamma = 4000$. The local pairing of the vortex tubes leads, in all of these cases, to the formation of vortex sheets.

Evolution at $\beta \gtrsim 67.4^\circ$ ($b \leq 3/2$) The evolution of the global quantities for runs 3, 6 and 7, all corresponding to $Re_\Gamma = 4000$, and $67.4^\circ \leq \beta \leq 90^\circ$ ($1 \leq b \leq 3/2$) is shown in Fig. 7. The initial value of the mean kinetic energy slightly increases with b , as shown in Fig. 7(a), and only decays by about 20% throughout the whole run, as it was the case at $\beta = 90^\circ$ (compare with Fig. 6). The main differences between the runs is indicated by the evolution of the mean dissipation rate and of $\langle \omega^6 \rangle^{1/3}$, as shown in Fig. 7(b-c). Namely, as β decreases, the time required for these plots to reach their respective maxima also decreases. Visualization studies, comparable to what has been done in the case $\beta = 90^\circ$, show that the peaks in Fig. 7(b-c) correspond to the time at which the vortices reconnect and the tubes change topology. Notably, the reconnection dynamics look comparable when $\beta = 90^\circ$ and $\beta \approx 77.3^\circ$ ($b = 5/4$), with the prominent formation of vortex sheets as illustrated in Fig. 4. The major difference between these two cases comes from the time at which the peaks develop, see Fig. 7(b-c). This difference can be qualitatively understood from the observation that when β decreases, the vortex tubes are initially closer to being antiparallel, and it therefore takes less time for them to locally align in an antiparallel manner and initiate the reconnection process. As explained earlier, this early phase can be captured with the Biot-Savart dynamics.

Contrary to the peaks of $\langle \omega^6 \rangle^{1/3}$ shown in Fig. 7(c), which are approximately constant, the peak energy dissipation rate is approximately twice as large for the configuration where $\beta \approx 67.4^\circ$ ($b = 3/2$) than for $\beta = 90^\circ$ ($b = 1$) or $\beta \approx 77.3^\circ$ ($b = 5/4$). Visualization in the former case also reveals the transient presence of vortex sheets when the tubes come together. The evolution, however, qualitatively differs from what was shown in Fig. 4, as the sheets do not stay close to one another. We view this regime as a transition towards the dynamics occurring at smaller values of β , which will be discussed in the following subsection.

C. Evolution at $\beta \leq 53.1^\circ$ ($b \geq 2$): short wavelength instability

As the initial condition is varied to increase the alignment of the tubes (i.e. $\beta \rightarrow 0$), the interactions close to the reconnection event become very different to what was shown for initially perpendicular tubes in Fig. 4. This is illustrated by Fig. 8, which shows the development of the interaction between the vortex tubes for run 11 with $\beta \approx 28.1^\circ$ ($b = 4$) and $Re_\Gamma = 4000$. Because the angle between the two tubes is much smaller than the initially perpendicular case ($b = 1$), the two tubes align, overlap, and interact over a significantly larger extent which is much larger than the initial vortex core size. This is clearly visible in the left column of Fig. 8, as the extent

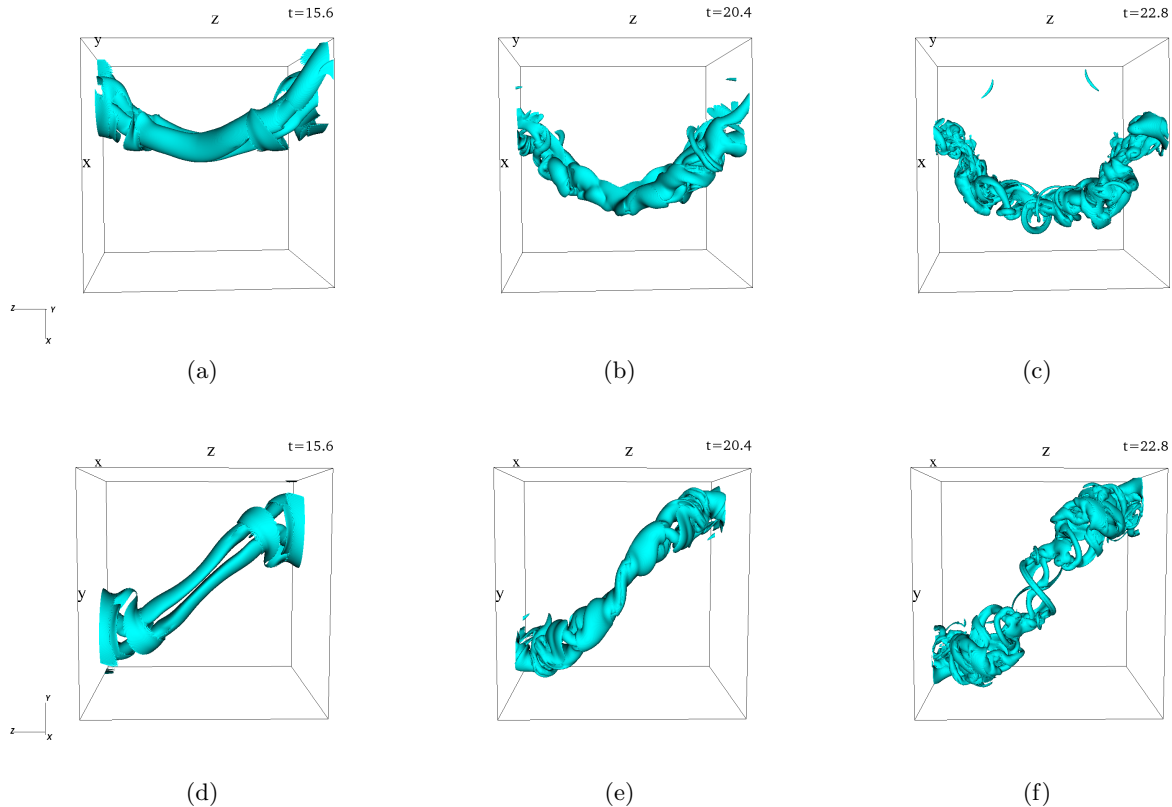


FIG. 8. Interaction and breakdown of nearly antiparallel vortex tubes. The evolution of the vorticity magnitude isosurface for run 11 ($\beta \approx 28.1^\circ$, $b = 4$, $Re_\Gamma = 4000$). Only a cubic subdomain, $[-2.6, 2.6]^3$, surrounding the regions where the vortices interact is shown. The isosurfaces of the vorticity field are shown at $t = 15.6$ (left), $t = 20.4$ (center) and $t = 22.8$ (right); the upper row shows the top view; and the bottom row shows the front view. The thresholds are $\omega_{thr} = 2.5$ ($t = 15.6$), 3.2 ($t = 20.4$) and 3.6 ($t = 22.8$). The latest time shown corresponds to the peak dissipation rate.

of the vortices in the z -direction is much larger than in the x - and y - directions. In fact, as the flow evolves from $t = 15.6$ (left column (a)) to $t = 20.4$ (central column), the vortices develop an instability over a wavelength comparable to the size of the core. As the instability further evolves, many small-scale vortices develop (c.f. the right panel of Fig. 8) through the mutual stretching and straining of perpendicular vortices which is mediated by the elliptical instability [24].

To characterize the development of the instability after $t \gtrsim 15.6$ and identify the means by which interacting tubes develop small-scale flow structures, clearly visible at $t = 20.4$ (in the middle column of Fig. 8), we tracked the centerlines of the tubes. Recall that the tubes are initially located on the (x, z) -plane and separated by a distance d in the y -direction, see Fig. 1. For small enough values of β , as the flow evolves, the tubes move primarily in the y - and x -directions as the vortex axis is almost parallel to the z direction. At each value of z along the axis of the tubes, we separate the y -domain into two subdomains, D_\pm , corresponding to the two tubes, as clearly visible from the front view at $T = 6.13$ in Fig. 8. In practice, this is done by computing the integral of ω^4 over x : $\zeta(y, z) = \int dx' \omega^4(x', y, z)$ and by identifying, at each position z , the value of y that separates the upper and lower part of the tube. We then determined the x -location of the centroids at each value of z by computing the moments $x_\pm = (\int_{D_\pm} dx dy \omega^4 x) / (\int_{D_\pm} dx dy \omega^4)$, with a similar definition for y_\pm . We note that this way of defining the location of the centerlines

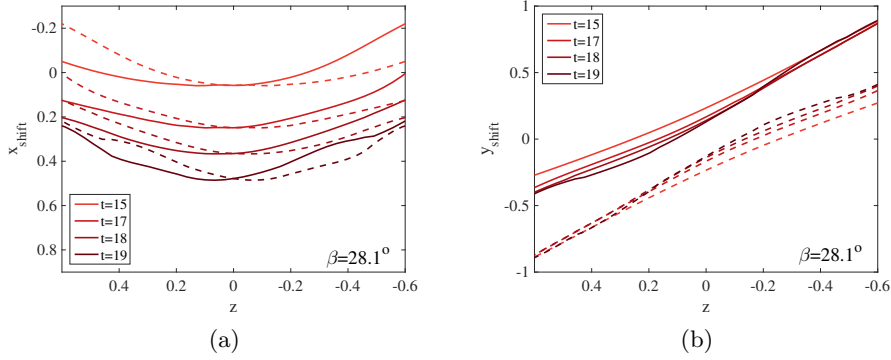


FIG. 9. Vortex centerline trajectories for nearly antiparallel vortex tubes for run 11 ($\beta \approx 28.1^\circ$, $b = 4$, $Re_\Gamma = 4000$). (a) Top view and (b) Side view. The solid lines correspond to the upper vortex and the dashed line correspond to the lower vortex. The centerlines were extracted by computing the moments of $\omega^4 x$, y and z . in a portion of the domain, including the central region where the vortices interact.

fails as the two tubes begin to interpenetrate, as shown at $t = 20.4$ in Fig. 8.

Fig. 9 shows the top (a) and front views (b) of the vortex tube centerlines; the full lines indicate the upper vortex, and the dashed lines indicate the lower vortex. The evolution of the centerline locations suggests the development of an instability with a wavelength comparable to the core radii. In terms of distinguishing between which vortex instability drives the growth of this perturbation—either the Crow instability [12] or the elliptic instability [46]—we are faced with the difficulty that the symmetry of the modes is not as clear as in the case of two initially parallel vortex tubes ($\beta = 0$), as found in [24]. This can be easily understood, given the relatively small size of the cores in interaction and the constraints on either side of the region of interaction. Nonetheless, the small distance between the cores, and the latest stage of the development shown in Fig. 9, where perpendicular filaments are formed, suggests the prevalence as time progresses of a symmetry that corresponds more to the elliptic instability, than to the Crow instability, reminiscent of what was observed in [24, 27].

The results shown in this subsection contrast sharply with those shown in Section III B for $\beta \gtrsim 67.4^\circ$ ($b < 3/2$). In fact, we can distinguish between two very different qualitative behaviors. For $\beta \gtrsim 67.4^\circ$, ($b < 3/2$), the interaction of the vortex tubes leads to the localized formation of thin vortex sheets that are limited to the interaction zone. In contrast, for $\beta \lesssim 53.1^\circ$, ($b \geq 2$), the interaction of the two vortex tubes leads to an interaction similar to that shown in Fig. 8, where perpendicular, fine-scale filaments arise throughout large areas of the domain. We stress the qualitative resemblance of the production of small-scales in this figure with the results shown in [24, 27]. We recall that the flow corresponding the run 7 ($\beta \approx 67.4^\circ$, $b = 3/2$) does lead to the development of sheets, but the interaction mechanism ultimately differs from those shown in Fig. 4 and in Fig. 8 because even if small-scale perpendicular filaments arise they come in small numbers and do not interact with each other significantly.

Fig.10 shows the time-dependence of the kinetic energy of the runs (panel a), the dissipation rate (b), and the 6th moment of vorticity, $\langle \omega^6 \rangle^{1/3}$ for runs 8-11, where $\beta \leq 53.1^\circ$ ($b \geq 2$) and $Re_\Gamma = 4000$. We have indicated by a cross in Fig. 10(b-c) the latest time corresponding to the visualization in Fig. 8(c), which approximately coincides with the peak dissipation rate. As was the case for the runs at $\beta \gtrsim 67.4^\circ$ ($b \leq 3/2$), see Fig. 7), the time of the peak dissipation, t_{peak} , varies with β . Fig. 10b shows that t_{peak} increases when β decreases. It should be kept in mind that the time at which the interaction occurs is a consequence of the pairing process, which depends on the

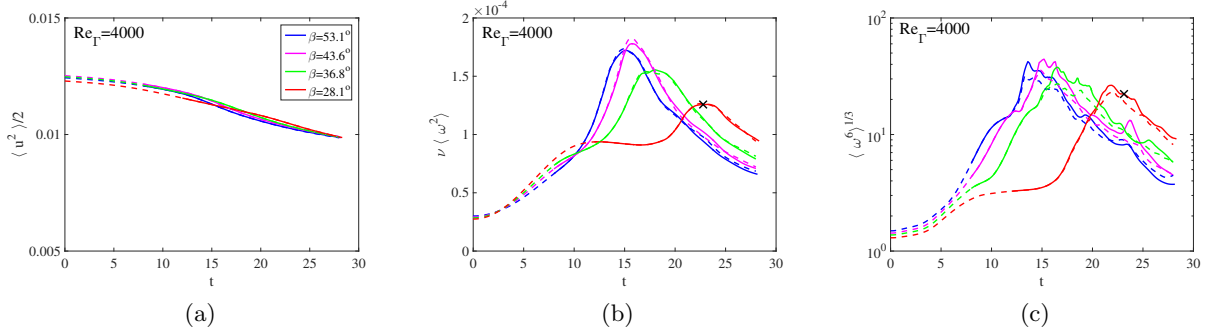


FIG. 10. Global dynamics for vortex tubes initially oriented at shallow angles. The evolution of (a) the mean kinetic energy rate, $\langle \mathbf{u}^2 \rangle / 2$, (b) the mean dissipation rate, $\nu \langle \omega^2 \rangle$, and (c) the mean 6th moment of the vorticity, $\langle \omega^6 \rangle^{1/3}$, for runs 8 ($\beta \approx 53.1^\circ$, $b = 2$), 9 ($\beta \approx 43.6^\circ$, $b = 5/2$), 10 ($\beta \approx 36.8^\circ$, $b = 3$), and 11 ($\beta \approx 28.1^\circ$, $b = 4$), at fixed $Re_\Gamma = 4000$.

precise geometry of the problem, and more specifically, on the angle β between the vortex tubes. As the tubes become more parallel, it takes a longer time for the interaction between the tubes to initiate. In the limit of perfectly antiparallel filaments, this time becomes the time necessary for instabilities to grow, as observed in [24]. It depends on the amount of noise initially, and it can be much longer than the time $t \approx 25$ for run 11 ($\beta \approx 28.1^\circ$, $b = 4$). In fact, we checked that the triggering of the elliptic instability, leading to the strong interaction between two antiparallel vortex tubes, is delayed when decreasing the amplitude of the noise added to the solution. This is consistent with the intuitive notion that the interaction leading to turbulence starts with an exponential growth of a small perturbation of the two initially antiparallel vortex tubes.

Interestingly, we also notice that the value of the peak dissipation rate tends to decrease when β decreases, for $\beta \lesssim 43.6^\circ$ ($b \gtrsim 5/2$). A similar trend is also observed in the 6th moment, see Fig. 10(c) as well as for the fourth and 8th moments (not shown). Contrary to runs at higher values of β , we observe a stronger difference between the runs at low resolution (with N_l Fourier modes, shown as dashed lines), and the runs at a higher resolution (with N_h Fourier modes, shown as full lines). This indicates stronger resolution requirements for these runs.

D. Discussion

Whereas the interaction between vortex tubes always leads to reconnection i.e. to a change of topology of the vortex lines, the mechanisms involved when the initial conditions are close to anti-parallel ($\beta \lesssim 33.7^\circ$ or $b > 3/2$, see subsection III C), appear to qualitatively differ from what is observed when the vortices are closer to being perpendicular ($\beta \gtrsim 33.7^\circ$ or $b < 3/2$) as discussed in subsection III B. The dynamics observed in the former case are very reminiscent of what was observed during the interaction of two initially antiparallel vortex tubes [24, 27]. The qualitative similarity between reconnection when $b = 4$, occurring through the annihilation of a large fraction of the two locally antiparallel tubes, clearly shown in Fig. 3 and 8 and the dynamics resulting from the collision between two vortex rings [24] is an important aspect of our work.

This configuration of two antiparallel tubes corresponds formally to $\beta \rightarrow 0^\circ$ ($b \rightarrow \infty$). In fact, the behaviors of the mean kinetic energy, dissipation rate, and 6th moment of vorticity in runs with initially weakly perturbed antiparallel vortex tubes, see Fig. 11, are very comparable to that shown for $\beta = 28.1^\circ$. The main difference is that the time at which the violent interaction leads to the breakdown of the vortex tubes and generation of fine-scale flow structures begins at later

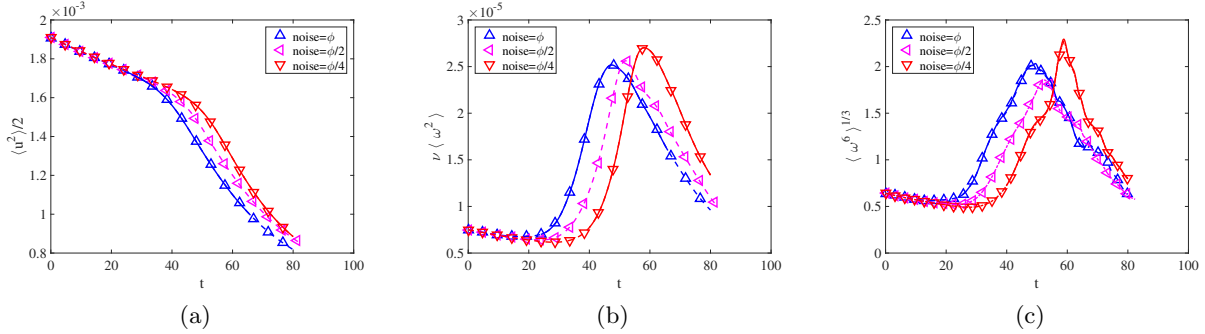


FIG. 11. Global dynamics for initially antiparallel vortex tubes with various noise levels. The evolution of (a) the mean kinetic energy rate, $\langle \mathbf{u}^2 \rangle / 2$, (b) the mean dissipation rate, $\nu \langle \omega^2 \rangle$, and (c) the mean 6th moment of the vorticity, $\langle \omega^6 \rangle^{1/3}$, for run 12 with varying noise amplitudes where $\beta = 0^\circ$ and $Re_\Gamma = 4000$.

times, compared to what is seen in Fig. 10(b-c). Furthermore, the time at which the interaction occurs depends on the level of noise. This can be clearly seen in Fig. 11(b-c), which compares 3 simulations with three different noise levels, obtained from a weak level (upward triangle symbols), half its value (left pointing triangles) and a quarter of its value (downward triangles). The time where the dissipation rate peaks clearly depends on the destabilization of the initial noise amplitude: we observe a logarithmic dependence of this time, consistent with the intuitive notion that the first stage of the interaction comes from the exponential growth of an unstable perturbation, through the elliptic instability.

This signals a clear qualitative difference between this configuration, where the interaction between the tubes leads to the annihilation of increasingly larger parts of overlapping tubes, and that obtained for $\beta > 67.4^\circ$ ($b < 3/2$), where intense, extremely thin vortex sheets form before a reconnection event [11, 17, 20]. Both types of event lead to the formation of small scale structures, albeit through different dynamics. We postulate that for sufficiently large Reynolds numbers and small values of β , reconnection is overtaken by the mutual annihilation of the two tubes through the elliptical instability. This is because the elliptical instability requires the strain to be aligned along the vortex core to begin to act (hence it barely acts for $\beta = 90^\circ$), but its growth rate is much larger than that of the Crow instability that leads to reconnection [24]. Even if the overall dynamics preceding reconnection appear to depend on the initial condition, the late stage of the interaction leads at high enough Reynolds numbers in all cases studied, to an intense generation of small-scales, plausibly through a cascade as demonstrated in the case of parallel tubes in [24]. It is tempting to postulate that this cascade through the generation of perpendicular, small-scale vortices, may in fact be universal [19, 42], independently of the initial conditions.

IV. SUMMARY AND CONCLUSION

In this work, we have investigated the interaction between two initially straight, counterrotating vortex tubes oriented at an angle β . We systematically varied β , hence the geometry of the initial flow configuration, and let the flow evolve. In all cases, we observe a change in topology of the vortex lines and the production of perpendicular small-scale vortices. The main result of our study is that the dynamics which result in this outcome depend strongly on the initial orientation of the interacting tubes.

When the tubes are initially almost perpendicular to each other ($\beta \approx \pi/2$), the interacting vortex tubes locally contact where they overlap, flattening into a pair of intense, slender vortex

sheets. This resembles the classically studied reconnection, found in the case of a pair of straight vortex tubes with a perturbation symmetric with respect to the plane separating the two vortices [11, 15–20, 39, 40], and which involves the flattening of the vortex tubes into intense, slender vortex sheets on either side of the symmetry plane. The underlying symmetries in the flow appear to be consistent with the eigenmodes corresponding to the long-wavelength (Crow) instability [12], and can be adequately captured in a flow with imposed symmetries. The breakdown of the tubes ultimately leads to abundant formation of small scales, see also [20].

However, when the angle between the two filaments is initially acute, we observe a breakdown mechanism that is comparable to that of Refs. [24, 27], with the formation of abundant small-scale vortices perpendicular to the original tubes, which effectively transfers more energy to the small-scales. The anti-symmetric elliptical instability drives the dynamics in this case, resulting in a breaking of the underlying symmetries discussed above. Hence, this evolution cannot be captured by flows with an imposed symmetry.

It is interesting to contrast this study with the non-universal aspects of vortex reconnection in superfluids, documented in [33], which rest on the precise geometry of the filament pair when the vortices reconnect. The nonuniversality documented in the present work rests on the dynamics of the vortex cores, which are responsible for the onset and dynamics of the elliptic instability. The Reynolds number also appears to be an important parameter in the reconnection of vortex tubes in classical fluids, a flow parameter without an analog in superfluids.

While the early stages of vortex interactions do not appear to lead to a universal reconnection scenario, we observe that the interaction between two vortex tubes leads in seemingly different ways, to a proliferation of small scale flow structures. In the problem considered here, when $\beta \approx \pi/2$, the small scales form after the sheets have annihilated, as observed in [20]. When the tubes are better aligned in an antiparallel manner, the formation of small-scale vortex structures via a cascade occurs as soon as the vortices come together [24]. The idea that iterative mechanisms may lead to formation of a cascade has been suggested for theoretical reasons [19, 47]. Strong evidence for a cascade driven by a hydrodynamic instability, namely the elliptic instability, has been presented in the interaction of two vortex tubes. An interesting question for future work will be to understand whether the mechanism leading to the proliferation of small-scale vortices is universal, based on the physical mechanisms discussed in [24]. The possibility that such a cascade scenario may lead to a singularity, as already postulated [19, 47, 48] also deserves further attention.

Acknowledgments: R.O.M. thanks the Research Computing Data Core (RCDC) at the University of Houston for providing computing resources. This research was funded by the National Science Foundation through the Harvard Materials Research Science and Engineering Center DMR-2011754, and through the Division of Mathematical Sciences DMS-1715477. M.P.B. is an investigator of the Simons Foundation. A.P. acknowledges financial support from the IDEXLYON project (Contract ANR-16-IDEX-0005) under University of Lyon auspices, as well as from the project TILT from ANR.

-
- [1] P. G. Saffman, “Dynamics of vorticity,” *J. Fluid Mech.* **106**, 49–58 (1981).
 - [2] P. R. Schatzle, *An experimental study of fusion of vortex rings*, Thesis, California Institute of Technology (1987).
 - [3] P. G. Saffman, *Vortex Dynamics* (Cambridge University Press, 1992).
 - [4] S. Goto, “Coherent structures and energy cascade in homogeneous turbulence,” *Progress of Theoretical Physics Supplement* **195**, 139–156 (2012).
 - [5] AKM Fazle Hussain, “Coherent structures and turbulence,” *Journal of Fluid Mechanics* **173**, 303–356 (1986).

- [6] M. W. Scheeler, W. M. van Rees, H. Kedia, D. Kleckner, and W. T.M. Irvine, “Complete measurement of helicity and its dynamics in vortex tubes,” *Science* **357**, 487–491 (2017).
- [7] G. K Batchelor, *An introduction to Fluid Dynamics* (Cambridge University Press, 1970).
- [8] A. Leonard, “Vortex methods for flow simulation,” *J. Comput. Phys.* **37**, 289–335 (1980).
- [9] E. D. Siggia, “Collapse and amplification of a vortex filament,” *Physics of Fluids* **28**, 794–805 (1985).
- [10] W. T. Ashurst and D. I. Meiron, “Numerical study of vortex reconnection,” *Phys. Rev. Lett.* **58**, 1632–1635 (1987).
- [11] A. Pumir and R. M. Kerr, “Numerical simulation of interacting vortex tubes,” *Phys. Rev. Lett.* **58**, 1636 (1987).
- [12] S. C. Crow, “Stability theory for a pair of trailing vortices,” *AIAA journal* **8**, 2172–2179 (1970).
- [13] E. D. Siggia and A. Pumir, “Incipient singularities in the Navier-Stokes equations,” *Phys. Rev. Lett.* **55**, 1749–1752 (1985).
- [14] A. Pumir and E. D. Siggia, “Vortex dynamics and the existence of solutions to the Navier-Stokes equations,” *Physics of Fluids* **30**, 1606–1626 (1987).
- [15] A. Pumir and E. D. Siggia, “Collapsing solutions to the 3d Euler equations,” *Physics of Fluids* **2**, 220–241 (1990).
- [16] M. J. Shelley, D. I. Meiron, and S. A. Orszag, “Dynamical aspects of vortex reconnection of perturbed antiparallel vortex tubes,” *J. Fluid Mech.* **246**, 613–652 (1993).
- [17] R. M. Kerr, “Evidence for a singularity of the three-dimensional incompressible Euler equations,” *Physics of Fluids A* **5**, 1725–1746 (1993).
- [18] T. Y. Hou and R. Li, “Dynamic depletion of vortex stretching and non-blowup of the 3-d incompressible Euler equations,” *J. Nonlinear Sci.* **16**, 639–664 (2006).
- [19] M. P. Brenner, S. Hormoz, and A. Pumir, “Potential singularity mechanism for the Euler equations,” *Phys. Rev. Fluids* **1**, 084503 (2016).
- [20] J. Yao and F. Hussain, “A physical model of turbulence cascade via vortex reconnection sequence and avalanche,” *J. Fluid Mech.* **883**, A51–1–36 (2020).
- [21] S. Hormoz and M. P. Brenner, “Absence of singularity of interacting vortex filaments,” *J. Fluids Mech.* **707**, 191–204 (2012).
- [22] H.K. Moffatt and Y. Kimura, “Towards a finite time singularity of the Navier-Stokes equations part 1. derivation and analysis of dynamical systems,” *Journal of Fluid Mechanics* **861**, 930–967 (2019).
- [23] W. M. van Rees, F. Hussain, and P. Koumoutsakos, “Vortex tube reconnection at $Re = 10^4$,” *Phys. Fluids* **24**, 075105 (2012).
- [24] R. McKeown, R. Ostilla-Mónico, A. Pumir, M. P. Brenner, and S. M. Rubinstein, “Turbulence generation through an iterative cascade of the elliptical instability,” *Science Advances* **6**, eaaz2717 (2020).
- [25] T.T. Lim and T.B. Nickels, “Instability and reconnection in the head-on collision of two vortex rings,” *Nature* **357**, 225–227 (1992).
- [26] T. Leweke, S. Le Dizès, and C. H.K. Williamson, “Dynamics and instabilities of vortex pairs,” *Annual Review of Fluid Mechanics* **48**, 507–541 (2016).
- [27] R. McKeown, R. Ostilla-Mónico, A. Pumir, M. P. Brenner, and S. M. Rubinstein, “A cascade leading to the emergence of small scale structures in vortex ring collisions,” *Phys. Rev. Fluids* **3**, 124702 (2018).
- [28] C. Y. Tsai and S. E. Widnall, “The stability of short waves on a straight vortex filament in a weak externally imposed strain field,” *Journal of Fluid Mechanics* **73**, 721–733 (1976).
- [29] D. W. Moore and P. G. Saffman, “The instability of a straight vortex filament in a strain field,” in *Proceedings of the Royal Society of London A: Mathematical, Physical and Engineering Sciences*, Vol. 346 (The Royal Society, 1975) pp. 413–425.
- [30] B. J. Bayly, “Three-dimensionality of elliptical flow,” *Phys. Rev. Lett.* **57**, 2160 (1986).
- [31] R. R. Kerswell, “Elliptic instabilities,” *Annu. Rev. Fluid Mech.* **34**, 83–113 (2002).
- [32] M.G. Linton, R. B. Dahlburg, and S. K. Antiochos, “Reconnection of twisted flux tubes as a function of contact angle,” *ApJ* **555**, 905–921 (2001).
- [33] A. Vilhois, D. Proment, and G. Krstulovic, “Universal and nonuniversal aspects of vortex reconnections in superfluids,” *Phys Rev Fluids* **2**, 044701 (2017).
- [34] Y. Kimura and H. K. Moffatt, “Reconnection of skewed vortices,” *Journal of Fluid Mechanics* **751**, 329–345 (1994).
- [35] C. L. Fefferman, “Existence and smoothness of the Navier-Stokes equation,” *The Millennium Prize problems*, 57–67 (2006).

- [36] O. Boratav, R. B. Pelz, and N. J. Zabusky, “Reconnection in orthogonally interacting vortex tubes: Direct numerical simulations and quantifications,” *Phys. Fluids* **3**, 581–605 (1992).
- [37] J. Yao, “Universal separation scaling for vortex reconnection in classical and quantum fluids,” *Bull. of the American Physical Society* (2020).
- [38] A. Pumir, “A numerical study of pressure fluctuations in three-dimensional incompressible homogeneous turbulence,” *Physics of Fluids* **6**, 2071–2083 (1994).
- [39] R. M. Kerr and A. K. M. F. Hussain, “Simulations of vortex reconnection,” *Physica D* **37**, 474–484 (1989).
- [40] R. M. Kerr, “The growth of vorticity moments in the Euler equations,” *Procedia IUTAM* **7**, 49–58 (2013).
- [41] See Supplementary Information at http://*** for supplementary videos.
- [42] S. Goto, Y. Saito, and G. Kawahara, “Hierarchy of antiparallel vortex tubes in spatially periodic turbulence at high Reynolds numbers,” *Phys. Rev. Fluids* **2**, 064603 (2017).
- [43] S. Kida and M. Takaoka, “Bridging in vortex reconnection,” *Phys. Fluids* **30**, 2911–2924 (1987).
- [44] M. V. Melander and F. Hussain, “Cut-and-connect of two antiparallel vortex tubes,” (Center for Turbulence Research, Stanford Univ., 1988).
- [45] S. Kida and M. Takaoka, “Vortex reconnection,” *Annu. Rev. Fluid Mech.* **26**, 169–189 (1994).
- [46] T. Leweke and C. H. K. Williamson, “Cooperative elliptic instability of a vortex pair,” *J. Fluid Mech.* **360**, 85–119 (1998).
- [47] T. Tao, “Finite time blowup for an averaged three-dimensional Navier-Stokes equation,” *Journal of the American Mathematical Society* **29**, 601–674 (2016).
- [48] J. Yao and F. Hussain, “On singularity formation via viscous vortex reconnection,” *J. Fluid Mech.* **888**, R2–1–12 (2020).